ACS Catalysis

Research Article

pubs.acs.org/acscatalysis

Unique Electrochemical Catalytic Behavior of Pt Nanoparticles Deposited on TiO_2 Nanotubes

Min Tian, Guosheng Wu, and Aicheng Chen*

Department of Chemistry, Lakehead University, 955 Oliver Road, Thunder Bay, Ontario P7B 5E1, Canada

ABSTRACT: In this study, we have directly deposited Pt nanoparticles on TiO_2 nanotubes (TiO_2/Pt) using a facile photoassisted reduction method. The Pt nanoparticles deposited on the TiO_2 nanotube arrays possess a large electrochemically active surface area and exhibit remarkable kinetic behaviors. The peaks for the oxide formation and reduction progressively decrease and eventually disappear completely after 800 cycles, whereas the integrated charge for hydrogen adsorption and desorption reaches a constant, ~70% of the initial value. In addition, an S-shaped cyclic voltammogram observed for the methanol oxidation at the electrochemically treated TiO_2/Pt electrode was dramatically different from the results obtained at a bulk Pt electrode. The self-refreshment functionality and anatomy of the reconstructed TiO_2-supported Pt nanoparticles described in this study provide a new approach for improving the catalytic activity of Pt nanomaterials in renewable energy applications.

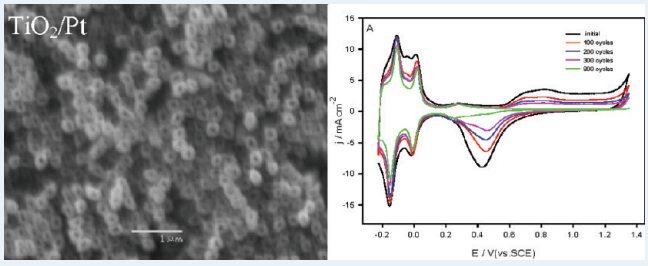

KEYWORDS: *TiO_2 nanotubes, Pt nanoparticles, photoreduction, methanol oxidation*

1. INTRODUCTION

Platinum plays an important role in the modern chemical and petrochemical industries, for automobile exhaust purification, and in the development of fuel cells due to its high catalytic activity and stability.[1−4] However, the large-scale expansion of fuel cell technologies has significantly increased the market price of Pt. It is therefore of vital importance to develop novel electrocatalysts that can utilize less Pt and provide higher activity. Nanostructured Pt catalysts have been attracting a great deal of attention in this regard.[5−7] Various approaches reported in the literature describe the fabrication of Pt-based nanostructures that have different dimensions and geometries: for instance, photochemical reduction,[8,9] chemical reduction,[10] sonochemical reduction,[11] and the hydrothermal method.[12,13]

Catalyst support technology has proven to be a very effective approach for improving Pt-based catalytic activity and for the reduction of Pt usage in catalysts, with the effect of lowering fuel-cell development costs. Supported Pt electrocatalysts are typically prepared by depositing or casting Pt nanoparticles, which are produced from the chemical reduction of H_2PtCl_6, on an amorphous carbon substrate. Alternatively, Ti and TiO_2 are promising support materials in catalyst development due to their high mechanical strength and chemical resistance.[14−17] Electronic interactions and synergetic effects between substrates and catalysts have also been reported.[18,19]

Fuels cells are complex electrochemical devices that produce clean energy by efficiently converting chemical energy to electrical energy through redox reactions. In particular, direct methanol fuel cells (DMFCs) are of great interest to many scientists because they possess a large power density. DMFCs also exhibit several advantages in comparison with other types of fuel cells, such as low operating cost, low operating temperature, the use of liquid fuel, and compactness.[20−23] However, the use of platinum as an electrocatalyst has the major disadvantage of CO poisoning, which greatly affects the performance of the electrode. Carbon monoxide inhibits the activity of Pt catalysts by strongly adsorbing to the electrode surface as a result of its formation as an intermediate of methanol oxidation.[24,25]

In the present work, we report on the unexpected and fascinating electrochemical performance of TiO_2-supported Pt (TiO_2/Pt) nanoparticles prepared by the photoassisted reduction of H_2PtCl_6 and treated by electrochemical cyclic sweep. The catalytic activity of the fabricated TiO_2/Pt nanoparticles was assessed by the electrochemical oxidation of methanol. For the first time, an S-shaped cyclic voltammogram was observed for methanol oxidation on electrochemically treated TiO_2/Pt nanoparticles, which is in dramatic contrast to the results obtained when using a bulk Pt electrode.

2. EXPERIMENTAL SECTION

2.1. Materials and Solutions. Solutions were prepared using sulfuric acid (Aldrich, 99.999%), methanol (Caledon, 99.9%), and pure water purified using a Nanopure water system (18.2 MΩ cm). Carbon monoxide (99.9%) was purchased from PRAXAIR. All solutions were deaerated with ultrapure argon (99.999%) prior to performing and measuring experiments, except the oxygen reduction experiments.

Received: December 28, 2011
Revised: February 3, 2012
Published: February 6, 2012

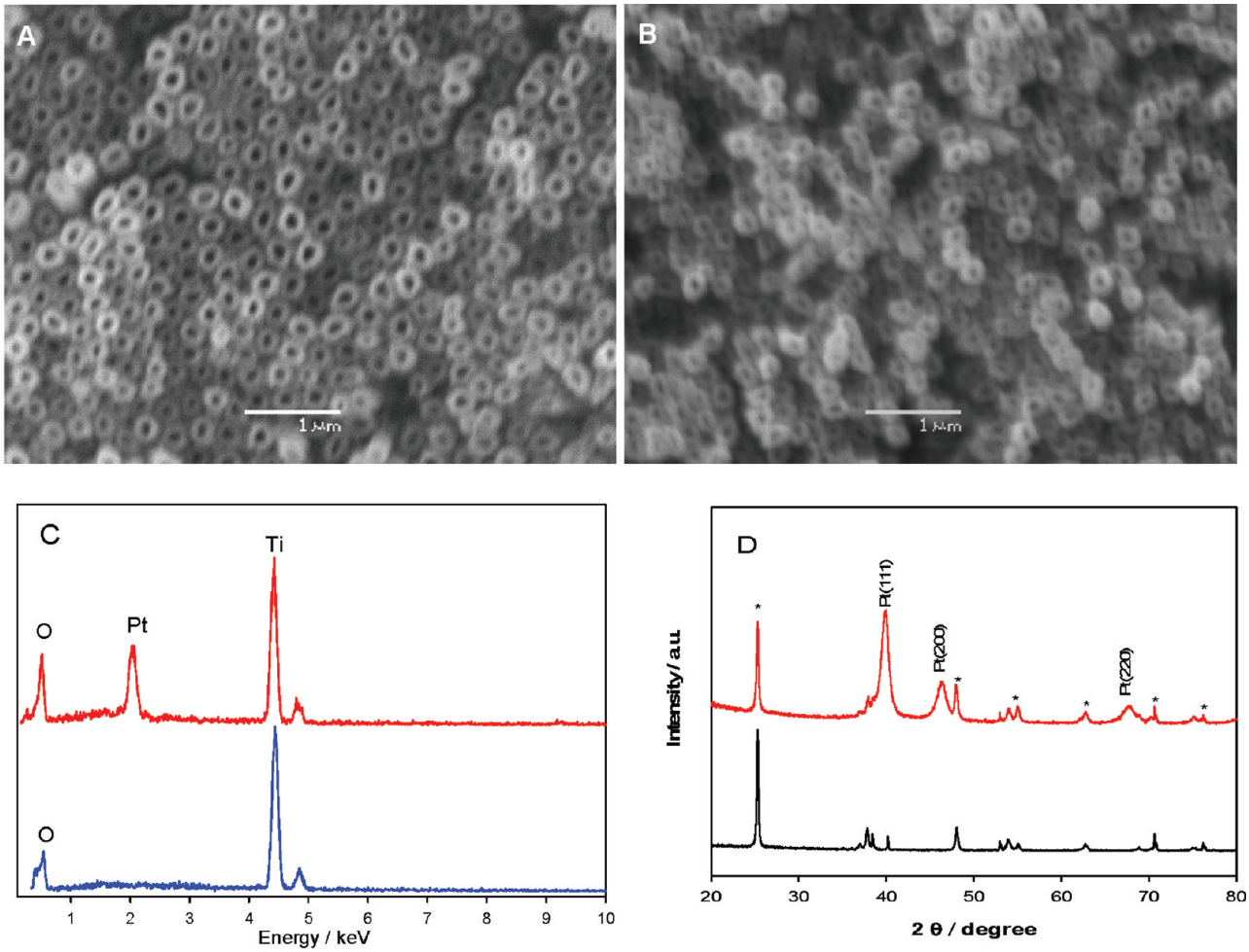

Figure 1. SEM images of (A) TiO_2 nanotubes, (B) TiO_2-supported Pt nanoparticles, (C) the corresponding EDS spectra, and (D) the corresponding XRD patterns. The peaks marked as stars are derived from the Ti substrate and the anatase phase of the TiO_2.

2.2. Fabrication of the TiO_2 Nanotubes and TiO_2/Pt Catalysts. The TiO_2 nanotube arrays were grown directly on titanium plates (1.25 cm × 0.8 cm × 0.5 mm, 99.2%, purchased from Alfa Aesar) using anodic oxidation. The Ti plates were initially sonicated in acetone, rinsed with pure water, and then etched in 18% HCl at 85 °C for 10 min to remove any oxides from the surface. The etched titanium plate was then submerged in a one-compartment, two-electrode cell containing DMSO + 2% HF and was electrochemically treated via anodization at 20 V for 24 h. To ensure that the anatase crystal structure of TiO_2 was obtained, the plates were annealed in an oven at 450 °C for 3 h.

The Pt nanoparticles were deposited onto the TiO_2 nanotubes from an aqueous solution of 2 mM $H_2PtCl_6 \cdot 6H_2O$ and 50% w/v methanol under UV light radiation. Exactly 40 μL of the above Pt precursor solution and 5 mL of 50% v/v methanol were added to a small quartz cell containing the TiO_2 electrode. The system was placed under a 150 W xenon arc lamp (LOT-Oriel GmbH & Co. KG, Germany) at room temperature for 30 min. Finally, the electrode was rinsed with pure water and dried for surface characterization and electrochemical study.

2.3. Characterization of the Synthesized TiO_2 Nanotubes and TiO_2/Pt Catalysts. The synthesized TiO_2 nanotube arrays and TiO_2-supported Pt nanoparticles were characterized by scanning electron microscopy (SEM) (JEOL 5900LV), X-ray diffraction (XRD) (Philips PW 1050-3710 diffractometer with Cu Kα radiation), and a Thermo Scientific Theta Probe X-ray photoelectron spectrometer (ThermoFisher, E. Grinstead, UK) and PicoSPM (Agilent Technologies). A three-electrode cell system was employed for the electrochemical studies. A Pt coil with a 10 cm^2 surface area was used as the auxiliary electrode, and a saturated calomel electrode (SCE) was used as the reference electrode. To enable a comparison to the TiO_2/Pt working electrodes, a 1 cm^2 polycrystalline Pt wire was also used as the working electrode. The electrochemical measurements were carried out at room temperature (20 ± 2 °C) using a Voltalab 40 Potentiostat (PGZ301).

3. RESULTS AND DISCUSSION

3.1. Characterization of the TiO_2/Pt Catalysts. The structure and morphology of the TiO_2 substrate and the photodeposited Pt nanoparticles were characterized by SEM. As shown in Figure 1A, the self-organized nanotubes consist of pored arrays with uniform diameters of ~80 nm. It is evident that the pore lumens are open at the top of the layer. The energy dispersive spectrum (EDS) of the nanotubes (the blue curve in Figure 1C) displays strong oxygen and titanium peaks, which confirms the composition of the formed TiO_2 nanotube arrays. Figure 1B presents a typical SEM image of the TiO_2/Pt electrode. The Pt nanoparticles are too diminutive to be

dx.doi.org/10.1021/cs200691a | ACS Catal. 2012, 2, 425–432

identified visually in the SEM image; however, a strong Pt peak in the EDS (the red curve in Figure 1C) confirms the presence of Pt deposited on the TiO_2 nanotubes.

Figure 1D presents the corresponding XRD patterns of the prepared TiO_2 nanotubes and TiO_2/Pt electrode. It is known that TiO_2 has two common phases—anatase and rutile—and that anatase TiO_2 exhibits higher photocatalytic activity than rutile TiO_2.[26,27] Except for the marked Pt peaks, all of the diffraction peaks are attributed to those of the tetragonal anatase TiO_2, revealing that the formed TiO_2 nanotubes exist in the anatase phase. This is beneficial for the process of photoassisted Pt deposition. The average crystal dimension of the Pt nanoparticles deposited on the TiO_2 nanotubes was estimated to be ~7.6 nm from the Scherrer formula.[28] The X-ray photoelectron spectrum (XPS) (not shown) shows two strong Pt ($4f_{7/2}$) and Pt ($4f_{5/2}$) peaks at 71.0 and 75.1 eV, respectively, further demonstrating the successful deposition of Pt nanoparticles on the TiO_2 nanotube arrays.

Figure 2A shows the photocurrent transients of the TiO_2 nanotube arrays, which were measured by switching a UV light source on and off in 0.5 M NaOH at an applied electrode potential of 0.6 V. The duration of the light pulses was set at 300 s, followed by dark current measurements for 120 s. As depicted in Figure 2A, the response of the photocurrent to the UV irradiation is rapid, with a value of ~5 mA cm^{-2}. The high photocurrent of the prepared TiO_2 nanotubes indicates that it is efficient to employ the photoassisted deposition method to modify the TiO_2 nanotube arrays with Pt nanoparticles.

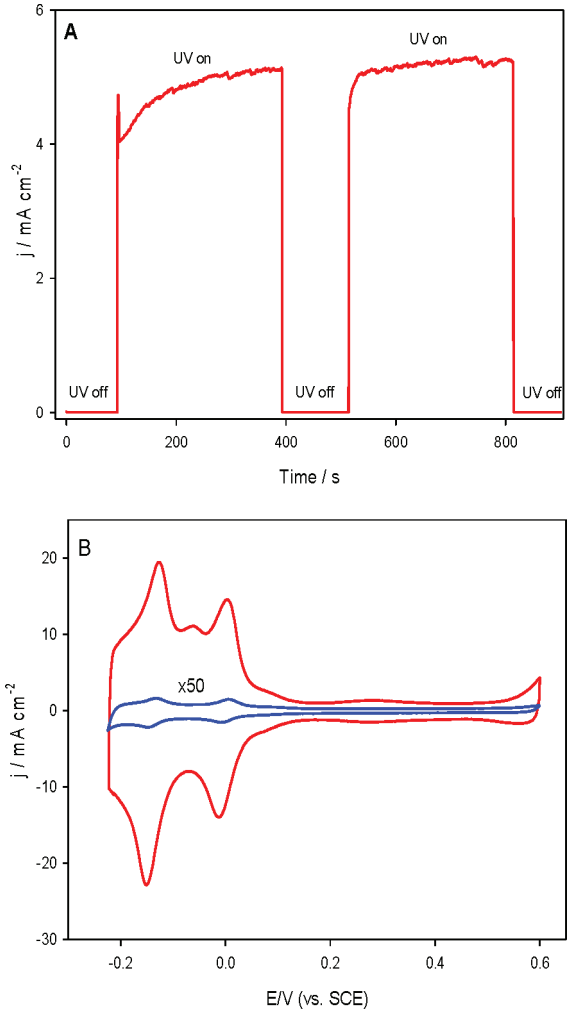

Figure 2. (A) Photocurrent of the prepared TiO_2 nanotubes measured in 0.5 M NaOH at applied potential bias 0.6 V. (B) Cyclic voltammograms for the TiO_2-supported Pt nanoparticles (red line) and polycrystalline Pt electrode (blue line) recorded in 0.5 M H_2SO_4 at a scan rate of 20 mV/s.

The electrochemically active surface area (ECSA) of a Pt electrode can be determined using hydrogen adsorption and desorption.[29] Figure 2B presents cyclic voltammograms (CVs) of hydrogen adsorption and desorption on the TiO_2/Pt electrode and a smooth polycrystalline Pt electrode for comparison. Both CVs display two strong peaks that appear in the potential range between −0.2 and 0.05 V in both the forward and reverse potential scans, which correspond to the typical profiles of hydrogen desorption and adsorption on the Pt electrode surface.[3,30,31] Assuming that the double-layer charging is constant in the entire scanned potential region, it is estimated that the integrated charge of the CVs presented in Figure 2B for hydrogen adsorption at the TiO_2-supported Pt nanoparticles is 116 mC cm^{-2}, which is over 500 times larger than that of the polycrystalline Pt surface (0.23 mC cm^{-2}). This indicates that the Pt nanoparticles deposited on the TiO_2 nanotube arrays possess a very large active surface area.

The ECSA was further investigated by utilizing the CO stripping experiment. The basic principle behind the use of CO adsorption and oxidation to determine the ECSA is similar to that involved with hydrogen adsorption and desorption. For comparison, Figure 3 presents the CVs for CO adsorption and oxidation on the TiO_2/Pt nanoparticles and the polycrystalline Pt electrode recorded in 0.5 M H_2SO_4. Prior to running the CVs, the potential was held at −0.1 V for 960 s during, which pure CO was purged into the electrolyte solution for the first 360 s. Pure Ar was then bubbled through the electrolyte for the remaining 600 s to ensure that the extra CO was completely removed from the solution. The first cycle displayed in Figure 3 shows a flat region between −0.2 and 0.1 V, where hydrogen

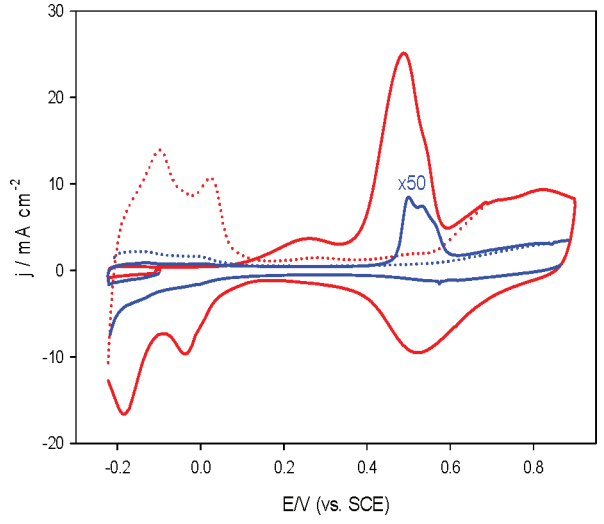

Figure 3. Cyclic voltammograms of CO oxidation during the first (solid line) and second cycles (dotted line) on the TiO_2/Pt electrode (red) and the polycrystalline Pt electrode (blue) recorded in 0.5 M H_2SO_4. Potential was scanned from −0.225 to 0.9 V at a scan rate of 20 mV/s.

dx.doi.org/10.1021/cs200691a | ACS Catal. 2012, 2, 425–432

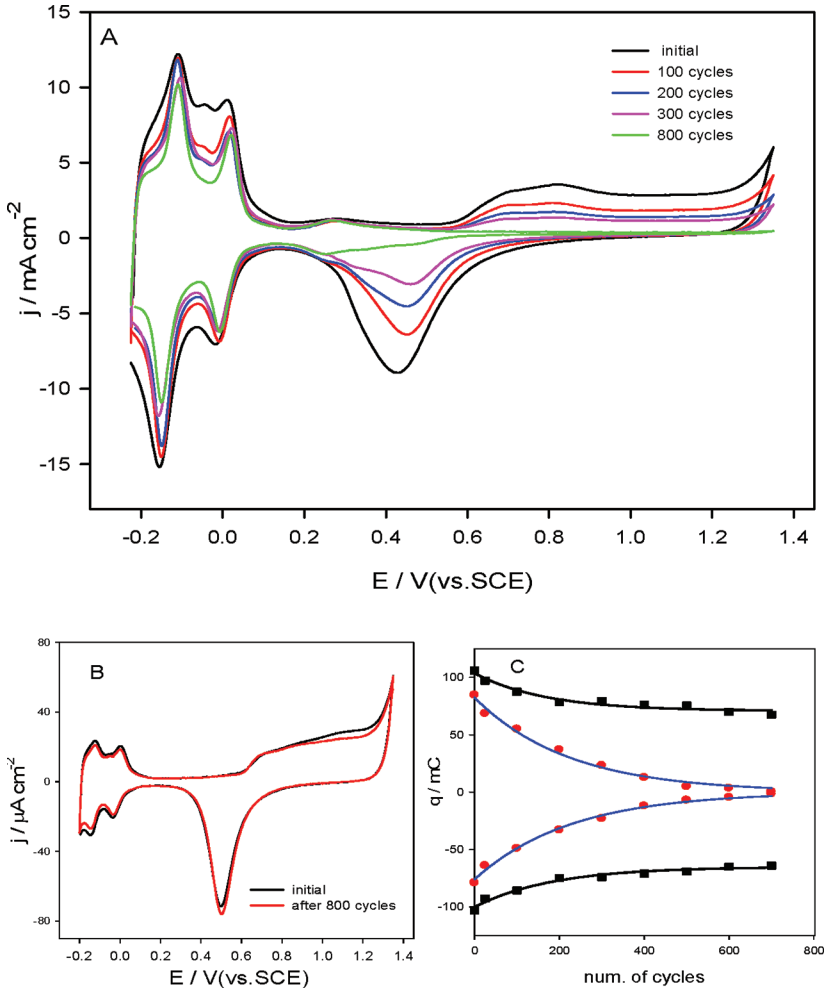

Figure 4. Representative cyclic voltammograms of (A) the TiO_2/Pt electrode and (B) polycrystalline Pt recorded in 0.5 M H_2SO_4 at a scan rate of 20 mV/s. (C) The charge variations for hydrogen adsorption/desorption and Pt oxide formation/reduction versus the number of electrochemical cycles.

desorption usually takes place, which is a result of the adsorbed CO. The integrated CO oxidation charges are 163 and 0.32 mC cm^{-2} for the TiO_2/Pt electrode and the polycrystalline Pt, respectively, showing that the active surface area of the TiO_2-supported Pt nanoparticles is ~510 times larger than that of the polycrystalline Pt electrode. This is consistent with the ECSA results determined from the hydrogen adsorption and desorption, further demonstrating the inherently huge active surface area of the TiO_2-supported Pt nanoparticles. In addition, the onset potential for CO oxidation on the TiO_2/Pt electrode was significantly shifted, and a broad shoulder appeared at ~0.2 V, indicating that the TiO_2-supported Pt nanoparticles possess much higher electrocatalytic activity toward CO oxidation compared with the Pt electrode.

3.2. Intriguing Behavior of the TiO_2/Pt Electrodes during the Electrochemical Cycling. The catalytic properties of nanostructured Pt may be specifically tuned either by modifying the composition of the Pt-based material, which mediates the electronic structure, or by tailoring the geometry of the Pt nanostructures, which alters the atomic arrangement and coordination at the surface.[6,7] Figure 4A presents a series of CV curves of the TiO_2/Pt electrode recorded in 0.5 M H_2SO_4 at a sweep rate of 20 mV s^{-1} in the potential range of −0.225 and 1.35 V (SCE). For clarification, only the first, 100th, 200th, 300th and 800th cycles are displayed. As seen in the initial CV curve (black), the voltammogram shows the typical hydrogen adsorption/desorption in the potential range between −0.225 and +0.2 V and oxide formation/reduction at the high potential range, similar to polycrystalline Pt electrodes,[30,31] albeit with much higher current. It is interesting to note that the peak intensity for oxide formation and reduction decreases progressively, and the peak potential for oxide reduction shifts progressively to a more positive potential with an increase in the number of cycles, (e.g., up to 300). The peaks for oxide formation and reduction disappear completely after 800 cycles. Surprisingly, the two reversible peaks centered at ~0.02 and −0.12 V(SCE) for hydrogen adsorption/desorption decrease by only 15% and 20%, respectively. For comparison, we also carried out the experiment using a bulk polycrystalline Pt electrode under the same conditions. As shown in Figure 4B, the CV curves of the bulk polycrystalline Pt electrode are virtually identical to the initial CV curve after 800 cycles.

The charge variations for hydrogen adsorption/desorption and for the oxide formation/reduction on the TiO_2/Pt electrode versus the number of cycles are presented in Figure 4C. The integrated charge for oxide formation is equivalent to the integrated charge for oxide reduction; both decrease simultaneously with an increase in the number of cycles, to approach zero after 800 cycles. In contrast, the charge decrease for hydrogen adsorption and desorption is much slower than

dx.doi.org/10.1021/cs200691a | ACS Catal. 2012, 2, 425−432

that for oxide formation and reduction. After 400 cycles, the integrated charge for hydrogen adsorption and desorption attains a constant at ~70% of the initial value. To the best of our knowledge, this dramatic and intriguing electrochemical performance of Pt nanoparticles has never been previously reported.

3.3. Remarkable Electrochemical Behavior for Oxidation of Methanol at the TiO_2/Pt Electrode Pretreated Electrochemically for 800 Cycles. Figure 5 displays the CVs

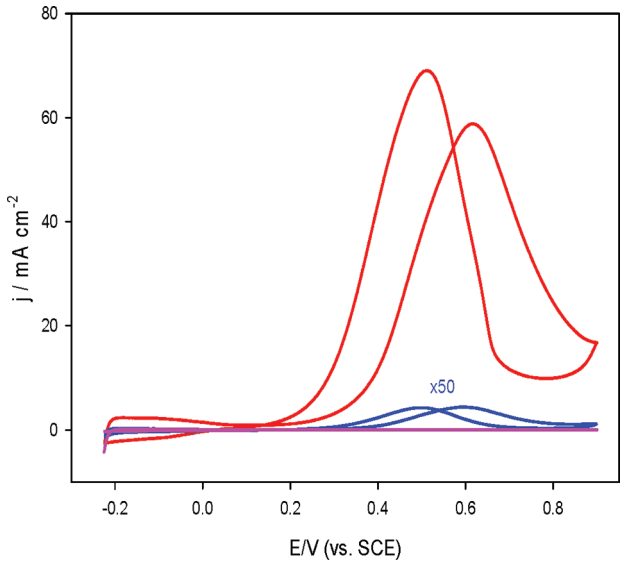

Figure 5. Cyclic voltammograms of methanol oxidation at the TiO_2/Pt electrode (red curve) compared with the polycrystalline Pt wire (blue curve) and TiO_2 (pink curve) in 0.1 M CH_3OH + 0.5 M H_2SO_4 with the potential scan rate at 20 mV/s.

of the TiO_2 nanotubes (pink curve), the polycrystalline Pt wire (blue curve), and the TiO_2/Pt electrode before the electrochemical cycling (red curve) recorded in 0.1 M CH_3OH + 0.5 M H_2SO_4 at a scan rate of 20 mV/s. As expected, no notable current was observed for methanol oxidation at the TiO_2 nanotubes. For clarification, the CV of the polycrystalline Pt electrode was magnified by 50 times. The electrochemical oxidation of methanol at the Pt wire and the TiO_2/Pt electrode exhibited two typical peaks: one located at 0.61 V in the forward scan and the other centered at 0.51 V in the reverse scan.

We further investigated the electrochemical activity of the TiO_2/Pt electrode toward methanol oxidation subsequent to being scanned for 800 cycles in 0.5 M H_2SO_4 at a sweep rate of 20 mV s^{-1} in the potential range of −0.225 and 1.60 V (SCE). As shown in Figure 6A, the electrochemically treated TiO_2/Pt electrode exhibits a dramatically different electrochemical behavior. The current of methanol oxidation on the treated TiO_2/Pt electrode remains constant at potentials above 0.6 V (SCE); an S-shaped curve is observed in the superimposed currents for both forward and backward potential sweeps. This is at complete variance with the CV curves from that before electrochemical treatment, polycrystalline Pt (Figure 5) and previous work,[6,9] in which two peaks were observed at 0.61 and 0.51 V (SCE) during the forward and backward sweeps, respectively. The ratio of current densities that are associated with the anodic peaks in the forward and reverse scan may be used to evaluate the tolerance of intermediates (e.g., CO).[1] The

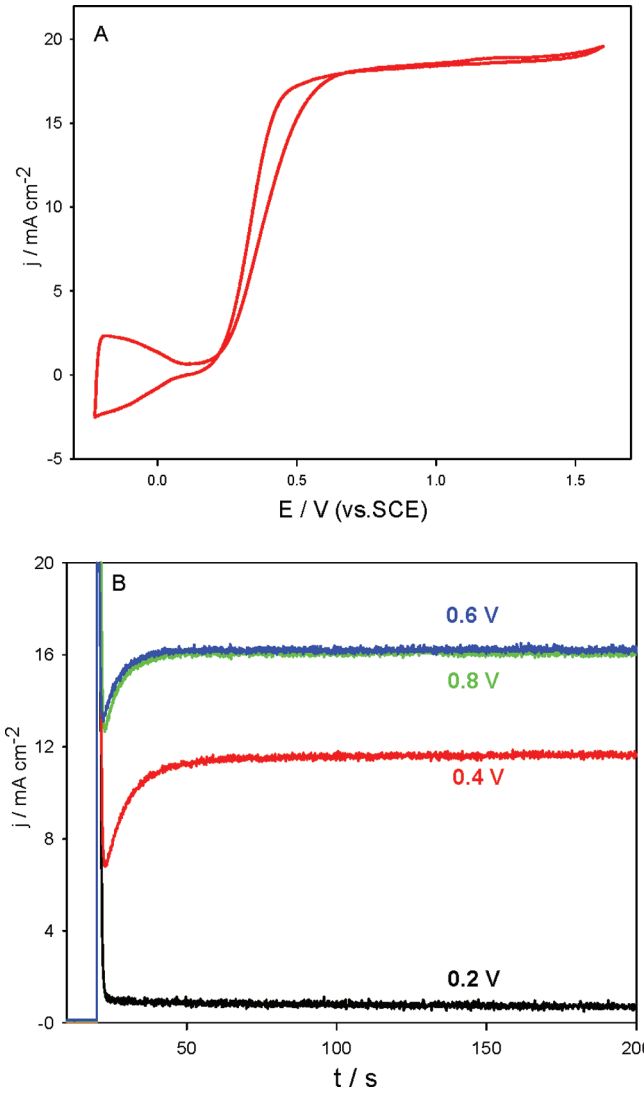

Figure 6. (A) Cyclic voltammograms of the electrochemically treated TiO_2-supported Pt nanoparticles recorded at a sweep rate of 20 mV/s. (B) Steady state current curves of the treated TiO_2-supported Pt nanoparticles measured at different electrode potentials. Electrolyte: 0.5 M H_2SO_4 + 0.1 M CH_3OH.

higher ratio values (~1.0) of the treated TiO_2/Pt electrode in the potential range of 0.6−1.6 V(SCE) indicate a significantly improved CO tolerance, which is desirable for DMFCs.

A chronoamperometric technique was employed to further compare the current densities for methanol oxidation at the electrochemically treated TiO_2/Pt electrode (Figure 6B). The initial potential was set at 0.0 V and then stepped to higher potentials and held for 5 min to reach the steady state value. As shown in Figure 6B, the current initially increased in the potential range of 0.2−0.6 V (SCE), and then became superimposed at the potential above 0.6 V (SCE), which is consistent with the CV results presented in Figure 6A.

To explore the causes of the interesting electrochemical performance of the electrochemically treated TiO_2/Pt electrode, we investigated the effect of the potential scan range. As displayed in Figure 7, the peaks for oxide formation and reduction decreased only when the upper limit sweep potential was higher than 0.8 V (SCE). At higher potentials, the Pt surface is oxidized and populated by oxygen species (O_{ad} and

dx.doi.org/10.1021/cs200691a | ACS Catal. 2012, 2, 425−432

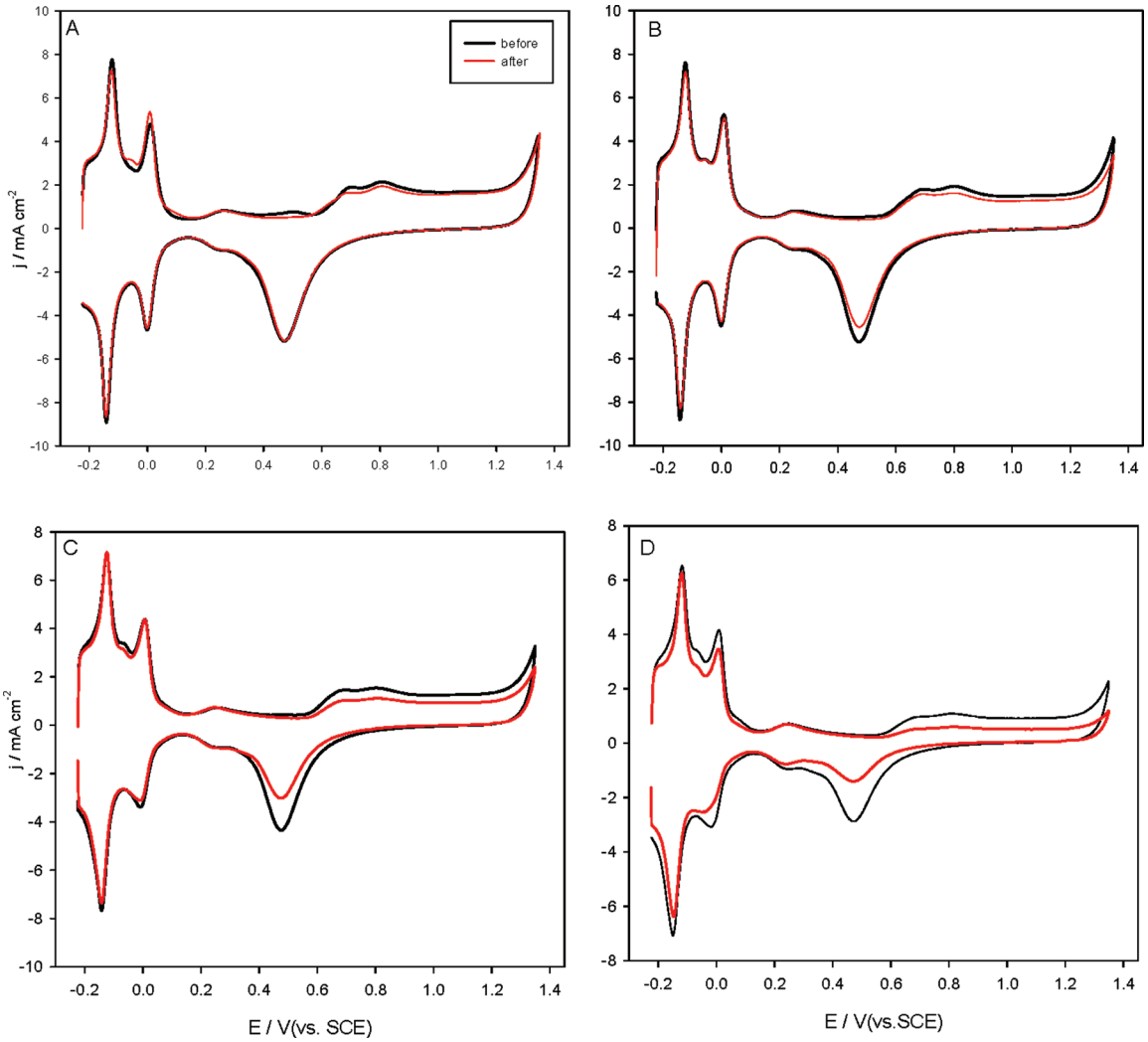

Figure 7. Cyclic volatmmogramms of the TiO_2-supported Pt nanoparticles in 0.5 M H_2SO_4 that were cycled for 200 cycles at differential sweep positive potential limits: (A) 0.8, (B) 1.0, (C) 1.2, and (D) 1.35 V, for which the negative potential limit was the same, −0.225 V. Scan rate (mV/s): 20.

OH_{ad}) that originate from the dissociation of H_2O in the solution.[30] The formed Pt oxide is then reduced at lower potentials during the sweeps. The oxidation of the Pt nanoparticles and the reduction of the formed Pt oxide were repeated via electrochemical cycling, resulting in the surface reconstruction of the Pt nanoparticles.[30] This is consistent with the recent discovery by Sun and co-workers,[7] in which platinum nanocrystals of an unusual tetrahexahedral shape were prepared via a square-wave electrochemical treatment of Pt nanoparticles that were supported on glassy carbon. This is further supported by our TEM analysis. Figure 8 presents TEM images of the initial Pt nanoparticles that were synthesized by photoassisted reduction (images A and C) and after being cycled in the potential range between −0.225 and 1.35 V for 800 cycles (images B and D), respectively.

The SAED patterns of the samples before and after the electrochemical treatment are also shown in the insets of Figure 8A and 8B, respectively. Two sets of diffraction patterns are observed in both of the SAED spectra. One set of diffraction patterns can be indexed to the (101), (103), (200), (105), and (213) planes of anatase phase TiO_2, and the other set of diffraction pattern can be attributed to the (111), (200), (220), and (311) planes of face-centered cubic Pt. As seen in the TEM images, the size of the Pt particles was around 5 nm in diameter.

After the electrochemical treatment, in addition to some large Pt particles, most particles became smaller, and their size was ∼2 nm in diameter, which is ∼2.5-fold smaller than that of the TiO_2-supported Pt nanoparticles before the treatment. This is also consistent with the CV studies shown in Figure 4A. After the electrochemical cycling, the peaks for hydrogen adsorption and desorption decreased. The remarkable and intriguing electrochemical performance of Pt nanoparticles deposited on the TiO_2 nanotubes for the oxide formation/reduction and the methanol oxidation might be attributed to (i) the surface reconstruction of Pt caused by the Pt oxide formation and reduction process;[7,31] (ii) the interaction of TiO_2 and Pt nanoparticles as observed at TiO_2/Au, showing that the TiO_2 substrate not only serves as a support to provide a means of spreading out Au particles over a large surface area, but also acts as a promoter for CO oxidation;[14,32] and (iii) the engagement of TiO_2 and the Pt oxide formed during the electrochemical cycling, which might stabilize the formed Pt oxide. As shown in Figure 4B, in the absence of TiO_2, the Pt oxide formed on the Pt polycrystalline electrode during the forward potential sweep was completely reduced in the course of the backward potential

dx.doi.org/10.1021/cs200691a | ACS Catal. 2012, 2, 425−432

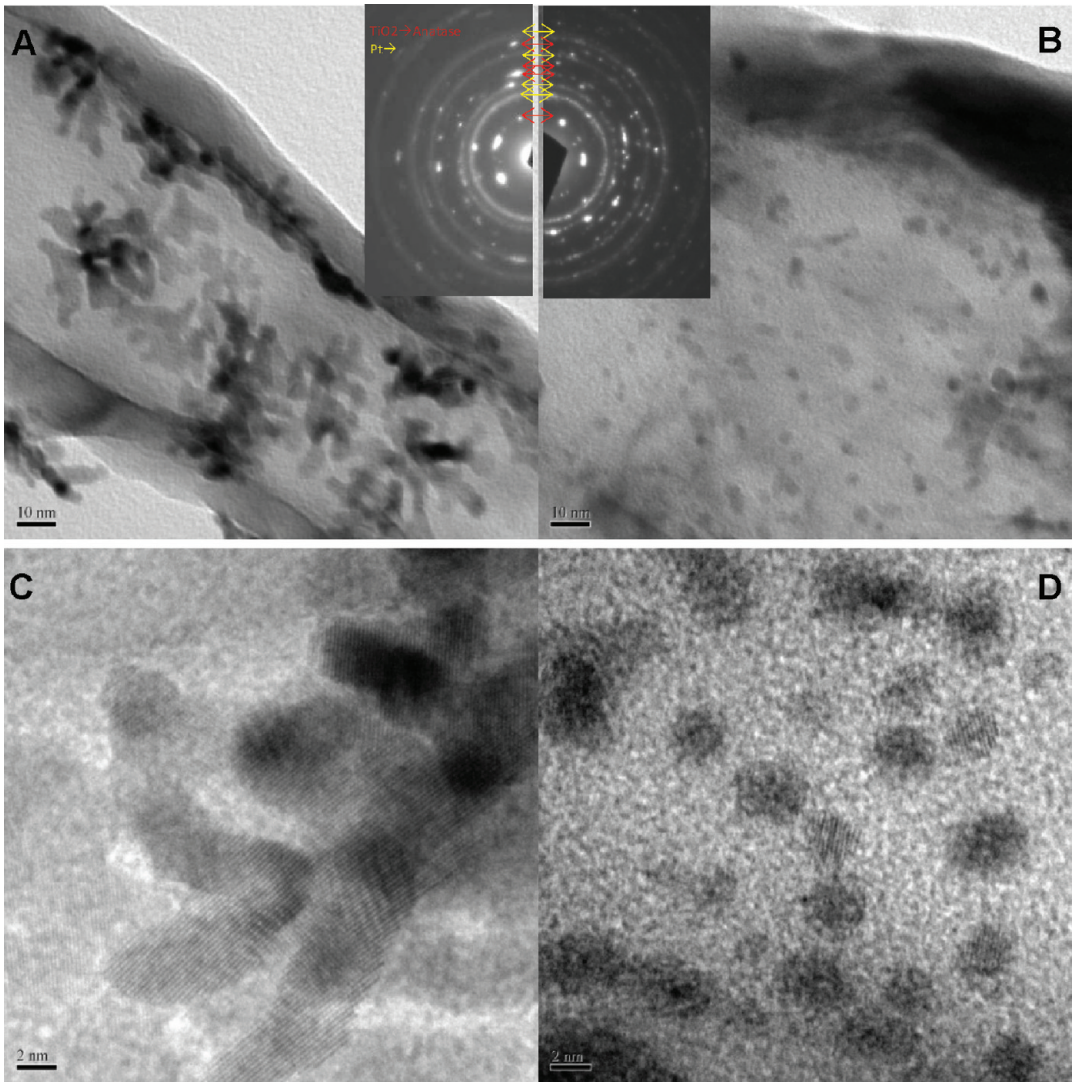

Figure 8. TEM images of TiO_2-supported Pt nanoparticles before (A, C) and after (B, D) the electrochemical treatment in 0.5 M H_2SO_4. Insets in A and B are the corresponding SAED spectra.

scan; thus no Pt oxide was accumulated during the electrochemical cycling. The engagement of TiO_2 and the Pt oxide might stabilize the formed Pt oxide, resulting in gradual accumulation of the Pt oxide and eventual disappearance of the formation and reduction of Pt oxide.

4. CONCLUSIONS

In summary, we have directly deposited Pt nanoparticles on TiO_2 nanotube arrays utilizing a facile photoassisted reduction method. The TiO_2-supported Pt nanoparticles possess a vast surface area that is over 500 times larger than that of a bulk polycrystalline Pt electrode. The TiO_2/Pt electrode exhibits a very high activity for the electrochemical oxidation of carbon monoxide and methanol. In addition, the TiO_2-supported Pt nanoparticles exhibit interesting kinetic behaviors in the formation and reduction of Pt oxide during electrochemical cycling, spanning the potential range between −0.225 and +1.35 V. The peaks for oxide formation and reduction incrementally decrease and then completely disappear after 800 cycles, whereas the integrated charge for hydrogen adsorption and desorption reaches a constant, ∼70% of the initial value. An S-shaped CV was observed for methanol oxidation on the electrochemically treated TiO_2/Pt electrode. The self-refreshment functionality and anatomy of the reconstructed TiO_2-supported Pt nanoparticles described in this study provide a new approach for improving the catalytic activity of Pt nanomaterials in renewable energy applications.

AUTHOR INFORMATION

Corresponding Author

*Fax:1-807-346-7775. E-mail: aicheng.chen@lakeheadu.ca.

Notes

The authors declare no competing financial interest.

ACKNOWLEDGMENTS

This work was supported by a Discovery Grant from the Natural Sciences and Engineering Research Council of Canada (NSERC). The authors thank Professor Zhonglin Wang and Dr. Yong Ding at the Georgia Institute of Technology for running TEM analysis. A.C. acknowledges NSERC and the Canadian Foundation of Innovation (CFI) for the Canada Research Chair Award in Materials and Environmental Chemistry.

REFERENCES

(1) Zhao, G. Y.; Li, H. L. *Appl. Surf. Sci.* **2008**, *254*, 3232.
(2) Abe, R.; Takami, H.; Murakami, N.; Ohtani, B. *J. Am. Chem. Soc.* **2008**, *130*, 7780.
(3) Tian, M.; Conway, B. E. *J. Electroanal. Chem.* **2008**, *616*, 45.
(4) Ahmadi, T. S.; Wang, Z. L.; Green, T. C.; Henglein, A.; El-Sayed, M. A. *Science* **1996**, *272*, 1924.
(5) Shao, M. H.; Peles, A.; Shoemaker, K. *Nano Lett.* **2011**, *11*, 3714.
(6) Chen, A.; Holt-Hindle, P. *Chem. Rev.* **2010**, *110*, 3767.
(7) Tian, N.; Zhou, Z. Y.; Sun, S. G.; Ding, Y.; Wang, Z. L. *Science* **2007**, *316*, 732.
(8) Song, Y. Y.; Gao, Z. D.; Schmuki, P. *Electrochem. Commun.* **2011**, *13*, 290.
(9) Bai, F.; Sun, Z. C.; Wu, H. M.; Haddad, R. E.; Xiao, X. Y.; Fan., H. Y. *Nano Lett.* **2011**, *11*, 3759.
(10) Chang, G.; Oyama, M.; Hirao, K. *Thin Solid Films* **2007**, *515*, 3311.
(11) Fujimoto, T.; Terauchi, S.; Umehara, H.; Kojima, I.; Henderson, W. *Chem. Mater.* **2001**, *13*, 1057.
(12) Koczkur, K.; Yi, Q.; Chen, A. *Adv. Mater.* **2007**, *19*, 2648.
(13) Wang, J.; Thomas, D. F.; Chen, A. *Chem. Commun.* **2008**, 5010.
(14) Tian, M.; Malig, M.; Chen, S.; Chen, A. *Electrochem. Commun.* **2011**, *13*, 370.
(15) Xie, Y.; Ding, K. L.; Liu, Z. M. *J. Am. Chem. Soc.* **2009**, *131*, 6648.
(16) Macak, J. M.; Barczuk, P. J.; Tsuchiya, H.; Nowakowska, M. Z.; Ghicov, A.; Chojak, M.; Bauer, S.; Virtanen, S.; Kulesza, P. J.; Schmuki, P. *Electrochem. Commun.* **2005**, *7*, 1417.
(17) Vijayan, B. K.; Dimitrijevic, N. M.; Wu, J. S.; Gray, K. A. *J. Phys. Chem. C* **2010**, *114*, 21262.
(18) Liu, Z. P.; Hu, P.; Alavi, A. *J. Am. Chem. Soc.* **2002**, *124*, 14770.
(19) Chen, A.; Russa, D. J. L.; Miller, B. *Langmuir* **2004**, *20*, 9695.
(20) Chen, M. H.; Jiang, Y. X.; Chen, S. R.; Huang, R.; Lin, J. L.; Chen, S. P.; Sun, S. G. *J. Phys. Chem. C* **2011**, *114*, 19055.
(21) Kuhn, M.; Napporn, T. W.; Meunier, M.; Therrlault, D. *J. Electrochem. Soc.* **2008**, *155*, B994.
(22) Chen, C.; Liu, D.; Huang, C.; Chang, C. *J. Power Sources* **2007**, *167*, 442.
(23) Cho, S. J; Ouyang, J. Y. *J. Phys. Chem. C* **2011**, *115*, 8519.
(24) Holt-Hindle, P.; Yi, Q.; Wu, G.; Koczkur, K.; Chen, A. *J. Electrochem. Soc.* **2008**, *155*, K5.
(25) Hepel, M.; Dela, I.; Hepel, T.; Luo, J.; Zhong, C. J. *Electrochim. Acta* **2007**, *52*, 5529.
(26) Tian, M.; Wu, G.; Adams, B.; Wen, J.; Chen, A. *J. Phys. Chem. C* **2008**, *112*, 825.
(27) Mohammadpour, R.; Irajizad, A.; Taghavinia, N.; Rahman, M.; Ahadian, M. M. *J. Mater. Sci. Technol.* **2010**, *26*, 535.
(28) Cullity; B. D., Ed.; *Elements of X-ray Diffraction*; Addison-Wesley Publishing Company: Reading, MA, 1967, p 514.
(29) Liu, Y.; Chen, J.; Zhang, W.; Ma, Z.; Swiegers, G. F.; Too, C. O.; Wallace, G. G. *Chem. Mater.* **2008**, *20*, 2605.
(30) Conway, B. E. *Prog. Surf. Sci.* **1995**, *49*, 331.
(31) Imai, H.; Izumi, K.; Matsumoto, M.; Kubo, Y.; Kato, K.; Imai, Y. *J. Am. Chem. Soc.* **2009**, *131*, 6293.
(32) Li, Z. P.; Gong, X. Q.; Kohanoff, J.; Sanchez, C.; Hu, P. *Phys. Rev. Lett.* **2003**, *91*, 266102.